Aeolian Research 33 (2018) 1–11

Contents lists available at ScienceDirect

Aeolian Research

journal homepage: www.elsevier.com/locate/aeolia

Determining sand strip characteristics using Argus video monitoring

P.M. Hage*, B.G. Ruessink, J.J.A. Donker

Department of Physical Geography, Faculty of Geosciences, Utrecht University, 3508TC Utrecht, The Netherlands

ARTICLE INFO

2010 MSC:
00-01
99-00

Keywords:
Aeolian sediment transport
Sand strips
Video monitoring
Beach processes
Transport conditions

ABSTRACT

The wind transports sand from the beach to the dunes and is therefore important for dune growth and recovery after a storm. Identifying the conditions that favour aeolian sand transport is especially important for narrow beaches, where measured long-term (seasons to years) deposition volumes on the foredune are often substantially less than the potential input from the beach. One of the most visually distinct signs of aeolian transport can be seen when relatively dry sand moves over a wet beach and organises itself to form low, slipfaceless bedforms. These features are known as sand strips. Here, we investigate the presence and characteristics of sand strips and their dependence on regional wind conditions by using a multi-year data set of video images of the Argus tower at Egmond aan Zee, The Netherlands. The dataset average wavelength and migration rate of the sand strips is 12.0 m and 1.24 m/h, respectively. Little to no relation was found between these two sand-strip characteristics and the wind velocity. The presence of these bedforms does not depend on wind velocity either, provided the wind velocity exceeds ~8 m/s. Instead, the wind direction determines if fully-developed sand strips form, as they are seen during alongshore or almost alongshore winds only. Our observations are indicative of topographic steering of the wind by the 25-m high foredune into the alongshore direction, as sand strips move alongshore even under onshore-oblique, regional winds.

1. Introduction

The intertidal beach is the primary source of the wind-blown sand needed for dune growth and/or recovery after an erosive storm event (e.g. Hoonhout and de Vries, 2017). However, knowledge of aeolian sediment transport on beaches is limited (e.g. Delgado-Fernandez, 2010), and most existing models have a tendency to overestimate sand deposition on the foredune (Miot da Silva and Hesp, 2010; Keijsers et al., 2014; Davidson-Arnott and Law, 1996). These models relate time-averaged sediment transport to wind shear velocity (Davidson-Arnott and Law, 1996; Bauer and Davidson-Arnott, 2002) and grain size (Sherman et al., 2013a). While this is realistic for a steady wind blowing over an unobstructed, horizontal surface with a uniform grain size (Gares, 1988; Sherman and Hotta, 1990; Bauer et al., 2009; Sherman and Li, 2012), transport on a natural beach is affected by, for example, the moisture content of the sand, the beach slope and the bed roughness (e.g. Delgado-Fernandez and Davidson-Arnott, 2011; Edwards and Namikas, 2009; Wiggs et al., 2004; Nield et al., 2013; Nield et al., 2014; Bauer and Davidson-Arnott, 2002; Svasek and Terwindt, 1974; Davidson-Arnott and Law, 1996; Jackson and Nordstrom, 1998; Sherman et al., 1998). Therefore, the moments with strong aeolian activity do not necessarily coincide with moments of high wind velocities (Delgado-Fernandez and Davidson-Arnott, 2011). Actual transport rates can be acquired through detailed field measurements (Sherman et al., 2017; Sherman et al., 2013b; Bauer et al., 2009; Davidson-Arnott and Bauer, 2009; Bauer and Davidson-Arnott, 2003; Udo et al., 2008; Davidson-Arnott et al., 2005; Jackson and Nordstrom, 1997; Baas and Sherman, 2006), however, most field campaigns on beaches concerning aeolian sediment transport are generally short in duration (ranging from minutes to weeks) and may therefore not contain the conditions that are most relevant to long-term (months to years) dune development (Delgado-Fernandez et al., 2009).

A suitable method for long-term measurements is video monitoring, which has already been used extensively to sample the wave-dominated part of the nearshore on timescales of years (van Enckevort et al., 2004; Ruessink et al., 2009; Pianca et al., 2015). Delgado-Fernandez et al. (2009) pioneered video monitoring to study aeolian transport. Their temporary camera system photographed the beach at Greenwich Dunes, Canada, at hourly intervals and occasionally picked up traces of aeolian sand transport during a nine-month period. Transported sand can be seen on video imagery because wind-blown sand usually is dryer and therefore lighter in colour than the moist bed, providing visual contrast. Additionally, the dry, transported sand can organise itself to form sand strips. These clearly visible, slipfaceless bedforms often form when a relatively moist bed is present (Bauer and Davidson-Arnott, 2002; Jackson et al., 2004; Davidson-Arnott et al., 2008; Bauer et al., 2009;

* Corresponding author.
E-mail address: P.M.Hage@uu.nl (P.M. Hage).

https://doi.org/10.1016/j.aeolia.2018.03.007
Received 10 January 2018; Received in revised form 14 February 2018; Accepted 9 March 2018

Nield et al., 2011; Nield, 2011), especially when vegetation (Sherman and Hotta, 1990; Eamer and Walker, 2010), frozen material (Hesp and Arens, 1997), or other roughness elements are present as well. Sand strips can grow into ephemeral dunes, which have a slipface and a height in the range of decimetres to a metre (Guimarães et al., 2016; Kocurek et al., 1992; Elbelrhiti, 2012), but waves and tides often destroy sand strips before they can grow this far. Video monitoring has been used to study ephemeral dunes on a long-term timescale by Guimarães et al. (2016). Like the traces of aeolian transport in the work of Delgado-Fernandez et al. (2009), these features were visible on camera because of a difference in moisture content, and therefore colour, between the transported sand of the bedforms and the bed (McKenna Neuman and Langston, 2006).

The most extensive field research into sand strips has been conducted by Nield et al. (2011), who have measured sand strip patterns with terrestrial laser scanning for a period of three and a half hours after a rain event. During this field experiment, sand transport increased as the beach surface dried, with erosion taking place at wet/dry surface boundary, and deposition further downwind (Nield and Wiggs, 2011). The patterns were later described in a cellular automaton model (Nield, 2011). According to the model, sand strip development is related to bed roughness, saltation and moisture patterns. The results gave rise to a conceptual model where the feedback between the surface properties and transport processes results in the development of bedforms at different spatial scales. Despite sand strips being common features in wet aeolian systems (Bauer and Davidson-Arnott, 2002; Jackson et al., 2004; Davidson-Arnott and Bauer, 2009), their behaviour under a wide range of wind conditions is largely unknown. The aim of this paper is to quantify the presence, length and migration velocity of the sand strips found at the beach of Egmond aan Zee, the Netherlands, using long-term video imaging, and to determine how these characteristics depend on regional wind conditions.

2. Study area

The study site is located between the beach towns of Egmond aan Zee and Castricum, the Netherlands (Fig. 1). The beach has a width varying between 30 and 100 m (depending on the tide) and is moderately sloping (1:30). The coastline is straight, with an orientation of 7° east of north. The sand has a median grain size of 240 μm. The intertidal beach typically contains one or two slipface bars (Masselink et al., 2006; Aagaard et al., 2005; Quartel and Grasmeijer, 2007). The foredune forms a uniform row parallel to the beach, with a height of 20–25 m. Its seaward front is steep (40–50°), due to occasional erosion events (de Winter et al., 2015). Most of the foredune is densely covered by European marram grass (*Ammophila arenaria*), especially at heights of 10 m and more above beach level.

The site experiences a semidiurnal tide with a range of 1.4 and 1.8 m during neap and spring tide, respectively, and is exposed to waves with directions between southwest and north. The annual significant offshore wave height and period along the Dutch coast are 1.2 m and 5 s, respectively, and show small alongshore differences (Wijnberg and Terwindt, 1995). During storms the offshore wave height can be over 5 m. Especially storms from the northwest are associated with surges in excess of 1 m, which can flood the intertidal beach for several days (Quartel et al., 2007). The dominant wind direction at this beach is south-southwest (210–230° with respect to north, Fig. 2), meaning the wind has a strong onshore-oblique character.

The beach of Egmond is monitored by an Argus video system (Enckevort and Ruessink, 2001), an optical remote sensing system pioneered by Holman and Sallenger (1986) to sample the nearshore environment. An Argus system consists of a suite of cameras mounted on a high structure, which provides an unhindered view on the beach. A timing module ensures synchronous camera collections (Holman and Stanley, 2007). The Argus system at Egmond aan Zee has five RGB-colour cameras, mounted on a 45-m high tower standing on the upper beach. The cameras provide an 180° alongshore view, from south-southwest to north-northeast. The Argus system was installed in April 1998. The image resolution was 640 × 480 pixels from 1998 to February 2004, 1024 × 768 pixels from 2004 to August 2005 and 1392 × 1040 pixels since then. Three different, oblique images are produced by each camera every thirty minutes: a snapshot, a time-exposure (timex) and a variance image. Only the first two types are used here. The timex images are created by averaging snapshots that are taken with a frequency of 2 Hz over a 10-min period. This blurs out movement that took place within those 10 min, such as individual waves breaking on the subtidal bars, people walking on the beach, and aeolian streamers.

The theoretical accuracy of the images is given by the footprint dimensions of individual pixels. The footprint, i.e. the projection of a

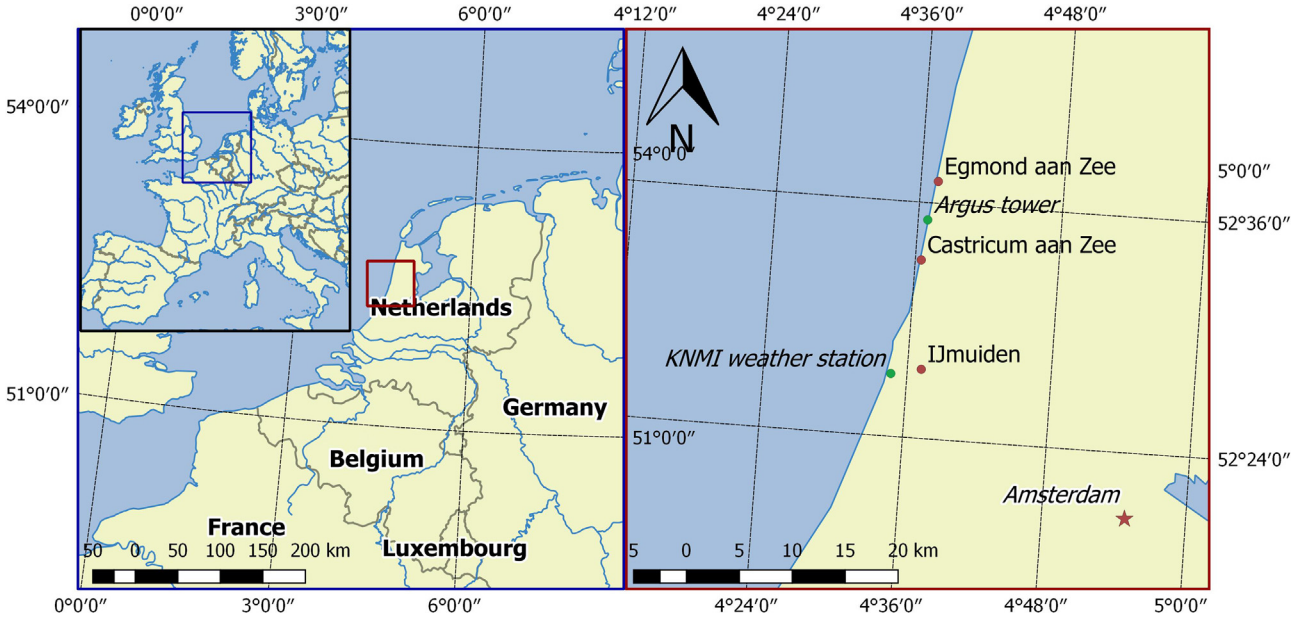

Fig. 1. Location of the field site and weather station.

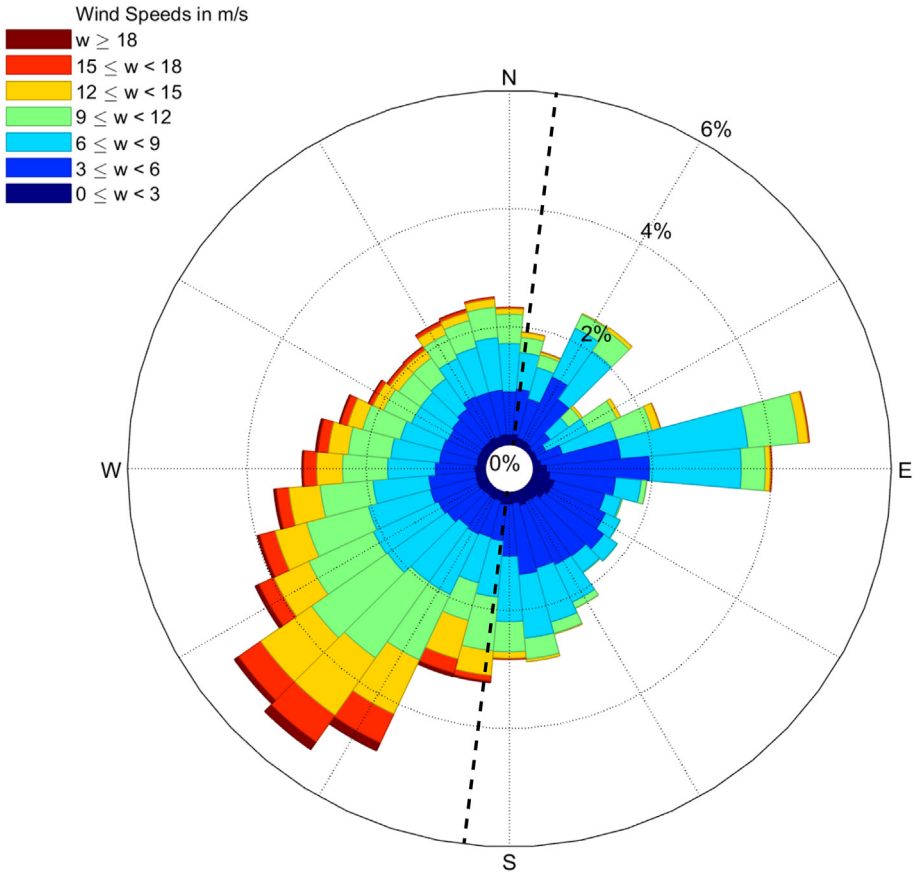

Fig. 2. Windrose, based on hourly wind speed U and direction θ data collected between 2005 and 2012 at IJmuiden, approximately 15 km south of our study site. The dotted line represents the orientation of the coast.

square image pixel on the ground, is near-rectangular with a generally larger alongshore than cross-shore side. Here, for the post-2005 system, the cross-shore footprint dimension is less than 0.2 m, while the alongshore size increases from 0.2 m at 100 m from the tower alongshore, to ≈1.5 m at 400 m.

This research uses the hourly mean wind velocity U and wind direction θ collected by a weather station in IJmuiden, roughly 15 km south of the field site (Fig. 1) as regional data. The weather data are made available by the Royal Netherlands Meteorological Institute (KNMI) with a resolution of 1 m/s for the U and 10° for θ. The anemometer is placed at a height of 10 m above ground level.

3. Methodology

The timex images from the Argus video system were used to study sand strip presence, occurrence, and behaviour. Finding images with sand strips manually is time-consuming, due to the vast size of the Argus database. Therefore, a first selection was made based on wind velocity. Sand transport can only take place when the wind velocity exceeds a certain threshold velocity. To this end, all Argus snapshots taken between October 2011 and March 2012 were studied to determine this threshold wind velocity. Snapshots were classified as having no, weak, or strong aeolian activity, based on the strength and number of visual signs of aeolian transport. Clear examples for each class can be found in Fig. 3. Aeolian activity was found predominantly for a wind speed in excess of 8 m/s, implying $U = 8$ m/s to be the threshold velocity. The images from 2005 to 2012 were filtered according to this threshold wind velocity, selecting only the days which had hourly mean wind velocities of 8 m/s or higher. Additionally, this threshold had to be surpassed for at least three hours to consider the wind transport event to be substantial for this site (Hage, 2014 to be found in https://dspace.library.uu.nl/handle/1874/301331).

Spatial correlation was, as described below, used to study the wave length and migration velocity of sand strips, but the Argus images must meet a number of conditions in order to perform correlation calculations. Firstly, the sand strips must be well-developed and active for at least one hour, meaning their appearance should not be patchy and their movement must be visible in subsequent images. Furthermore, the area containing them must be substantial in size, i.e. it must be at least 50 m long in the direction of the wind. Lastly, the sand strips have to be clearly visible, meaning rain, poor light conditions, or other circumstances that reduce image quality must be avoided.

The selected timex images were rectified and merged to make a plan view image as described by Holland et al. (1997) and Holman and Stanley (2007) (Fig. 4). The rectification involves the transformation from the two-dimensional (u,v) pixel coordinate scheme to the three-dimensional (x,y,z) real-world scheme, where x an y are horizontal coordinates and z is vertical elevation. Going from a 2D to a 3D coordinate system results in a system of equations that is underdetermined, but it can be solved by constaining z to a fixed value (Holland et al., 1997). In earlier Argus research that focussed on wave-breaking patterns, z was set to the tidal level (e.g. Lippmann and Holman, 1989). Because the sand strip patterns studied here were on the upper beach, z was set to 1 m above NAP (Amsterdam Ordnance Datum, with 0 m NAP corresponding to Mean Sea Level, MSL).

As aforementioned, the oblique nature of the original timex images causes the quality of the plan view images to diminish with distance from the Argus tower. Sand strips at Egmond are therefore visible only

Fig. 3. Examples of snapshots made by the north-facing camera and classified according to their visual signs of aeolian activity: no visual aeolian transport (A), some signs of aeolian activity, with small patches of relatively dry sand on a moist surface (B), strong signs of aeolian activity, where almost the entire beach is covered with sand strips (C). The wind conditions were: (A) $U = 9$ m/s, $\theta = -7^{\circ}$; (B) $U = 13$ m/s, $\theta = 37^{\circ}$; (C) $U = 16$ m/s, $\theta = 77^{\circ}$; where $\theta = 0^{\circ}$ is directed cross-shore from the west, $\theta = -90^{\circ}$ alongshore from the north, and $\theta = 90^{\circ}$ alongshore from the south.

if they are within a few hundred meters from the tower. For this study, the area transposed from oblique to plan view is 800 m alongshore (400 m at each side of the tower) and 300 m wide cross-shore (Fig. 5A). These plan view images were set to have a resolution of 0.5 × 0.5 m per pixel, meaning that the sand strips must migrate at least 0.5 m/h for their movement to be visible. The next step involved cutting out a small area containing well-developed sand strips from the 800 by 300 m plan view images and turning it greyscale (Fig. 5B) according to (ITU, 2011):

$$Greyvalue = 0.2989{*}R + 0.5870{*}G + 0.1140{*}B, \quad (1)$$

where R,G, and B are the pixelvalues for red, green, and blue, respectively. The cropped area had a size of approximately 25 m (cross-shore) by 100 m (alongshore) and covered a part of the upper beach with distinctive, well-developed sand strips, preferably close to the tower where the image quality is best. The exact size and location of the cropped area varied per day, since sand strips did not always develop at the same parts of the beach. The greyscale images were manually rotated before cropping to display the sand strips as vertical lines in the new, cropped image. Fig. 5C shows examples of the pixel values of the same pixel row of the three consecutive hours shown in Fig. 5A, after being detrended by computing the least-squares fit of a straight line and normalised to have a mean of 1. The pixel value increases with increasing pixel brightness. Because sand strips create a pattern of alternating dark (wet sand) and light (dry sand) colours, the pixel values of a horizontal pixel row give an approximately sinusoid signal.

Autocorrelation was used to calculate sand strip wave length in each pixel row. This technique compares two sequences to find their correlation at different lags, where one sequence is the original signal, and the other a copy of that original but with a lag. This was done with the pixel values for each horizontal pixel row of the cropped area according to:

$$r(\tau) = E[(X_m - \mu)(X_{m+\tau} - \mu)]/\sigma^2, \quad (2)$$

where r is the correlation coefficient, τ is the lag, E is the expected value operator, X_m is the pixel value at a certain distance m,μ the mean and σ^2 is the variance. By definition, $r(0) = 1$. Positive peaks for r are found when the corresponding lag matches with the wavelength or multitude of wavelengths of sand strips. At the lag of the positive peak closest to

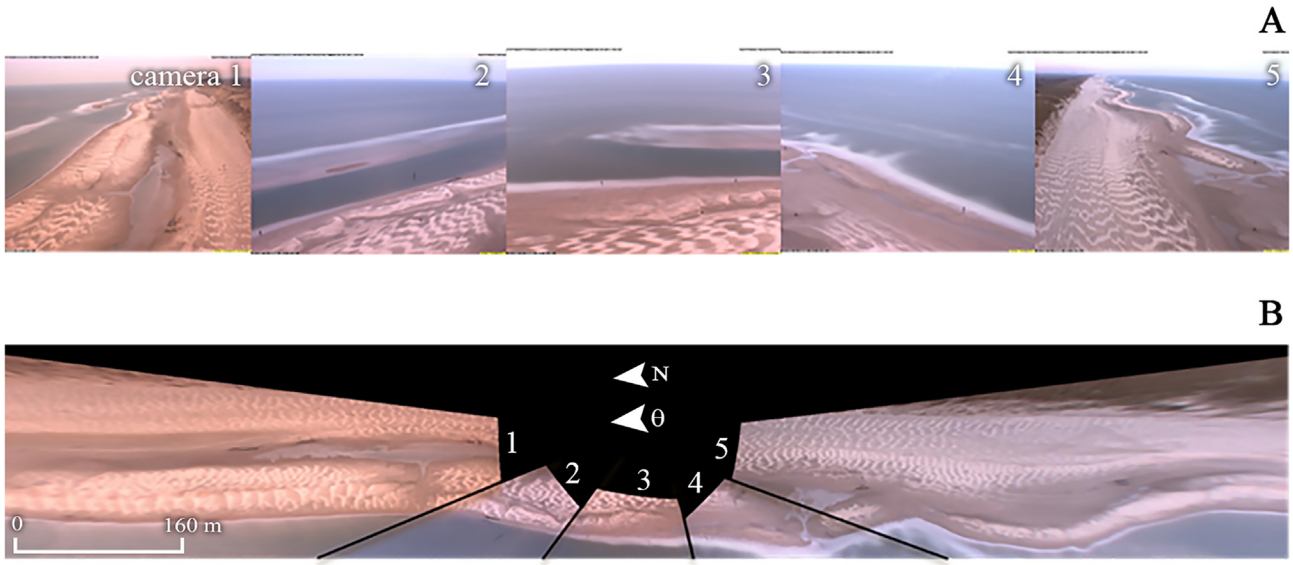

Fig. 4. The five original oblique Argus images (A) were rectified and merged to get a plan view image (B). Here, the plan view image has an alongshore and cross-shore length of 800 and 200 m. The example images were taken on 01-04-2008, The wind speed and direction were $U = 9$ m/s and $\theta = 97^{\circ}$ (i.e. almost alongshore). The arrows indicate the direction of the wind (θ) and the north (N). $\theta = 0^{\circ}$ is directed cross-shore from the west, $\theta = -90^{\circ}$ alongshore from the north, and $\theta = 90^{\circ}$ alongshore from the south.

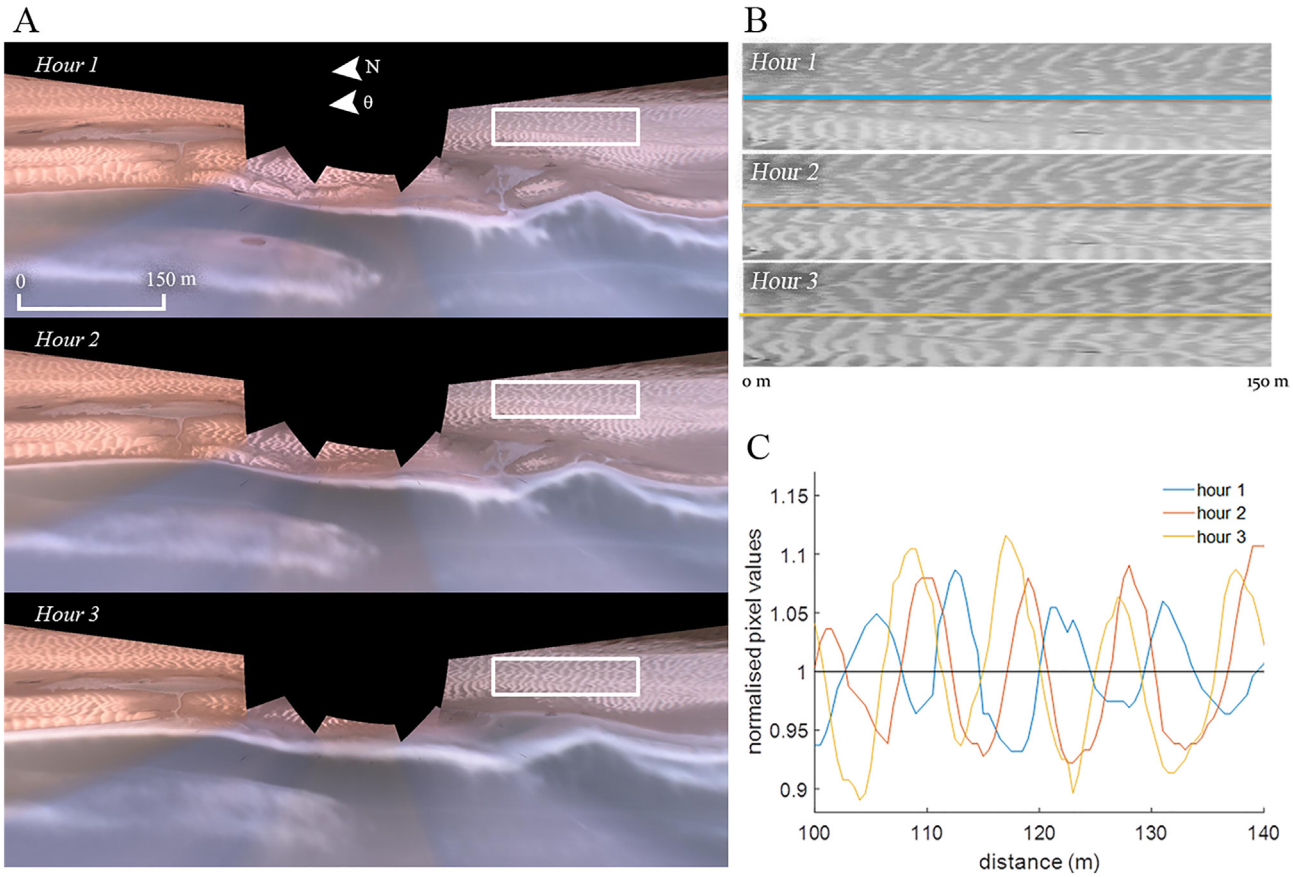

Fig. 5. Three plan-view Argus images made during consecutive hours that show well-developed sand strips (A). These images were cropped and turned to greyscale (B, boxes in A). The lines in (B) highlight the same horizontal pixel row in subsequent hours, whose normalised pixel values are plotted against alongshore distance (C). The normalised pixel values show a sinusoidal signal that shifts to the left with time, reflecting migration in northward direction. The example images were taken on 01-04-2008. The wind speed and direction were $U = 9$ m/s and $\theta = 97^{\circ}$. $\theta = 0^{\circ}$ is directed cross-shore from the west, $\theta = -90^{\circ}$ alongshore from the north, and $\theta = 90^{\circ}$ alongshore from the south.

$r(0)$, the pixel values of the sand strips of the original signal are compared with the pixel values of the neighbouring sand strips, giving the sand strips' wavelength in number of pixels. The lag corresponding to this peak was determined for each horizontal pixel row in each cropped image, as long as it surpassed a threshold of 0.3 for r. This threshold was chosen after comparing the lag of the first positive peak with its value for r for all pixelrows of all images used. Values for r below 0.3 result in a wide range of lags, which reflect highly irregular sand strips or may indicate a noisy signal. Meanwhile, an r above 0.3 gives lags focused around a central value that seems to be more realistic for the wavelength of sand strips. Results that seemed to be a multiple of this central value were ignored. An example of the selected lags for each pixelrow of a single hour can be found in Fig. 6, which shows that no lag was selected when a pixelrow did not have an r above the threshold of 0.3. The selected lags of the images part of the same sand strip event (subsequent hours during which sand strips are active) were averaged. This gives a mean wavelength in metres per sand strip event when multiplied with the 0.5 m pixel resolution.

The method for determining the migration velocity of the sand strips is similar to the one used for determining the wavelength. The same cropped area was used, but instead of using autocorrelation on the horizontal pixel rows, cross-correlation was used. Here, the pixel value signal of two subsequent hourly timex images were compared to each other. The lag with the first peak in the correlation represents the distance that the sand strips have moved, while the sign of the lag reflects migration direction. The minimal value for this correlation peak was 0.6, which was chosen in a similar manner as the 0.3 threshold for r for the sand strip wavelength calculations. At rare occasions, the highest correlation peak for a single pixelrow can be found at a lag that is upwind. As sand strips are not very likely to move in this direction, these outcomes were ignored. Unrealistically high lags, where the migration velocity was higher than its corresponding wavelength minus the standard deviation of the wavelength, were ignored as well, because these outcomes are more likely to represent the wavelength of the strips instead of their migration velocity. As with the wavelength of sand strips, the mean migration velocity per sand strip event was calculated by averaging over all rows and images.

4. Results

The conditions needed for visual traces of aeolian transport were investigated, using the Argus snapshot images taken between October 2011 and March 2012. Hours with any visual form of aeolian transport had, as aforementioned, wind velocities above ≈8 m/s and could be found for all wind directions, but showed a strong peak around south-westerly winds and a smaller one around north-westerly winds (Fig. 7). This corresponds to the wind climate at the field site. Visually strong aeolian activity, which includes well-developed sand strips, was found predominantly when the wind blew (almost) alongshore. The wind velocity during hours with strong signs of aeolian transport is not

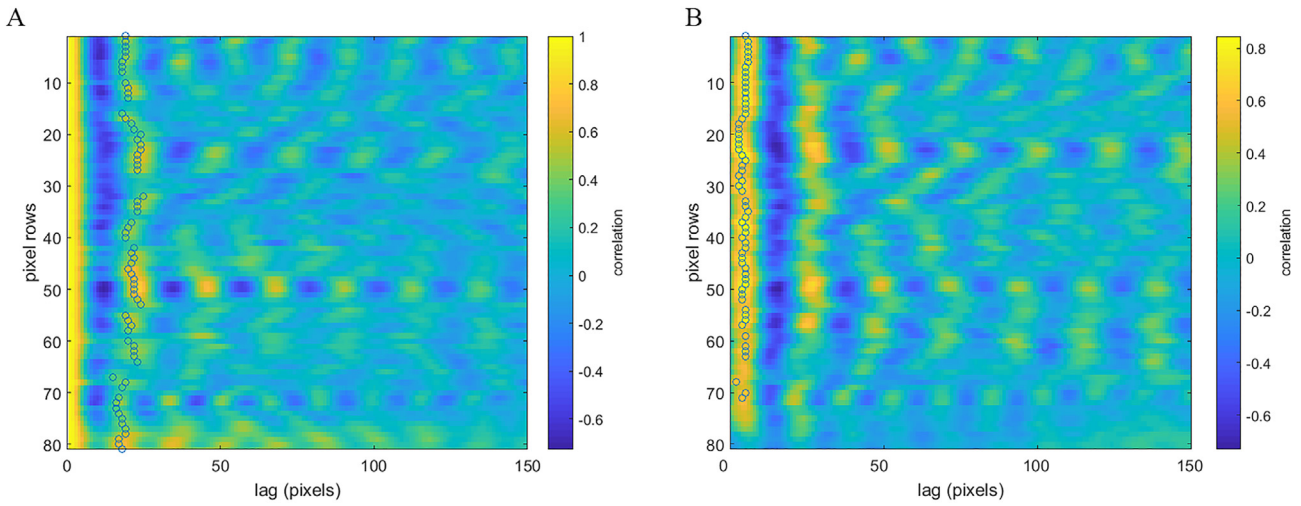

Fig. 6. Example of the correlation coefficients for the sand strip wavelength (A) and migration velocity (B), calculated for different lags for each pixelrow of the cropped area in Fig. 5. The pixelrows are orientated parallel to the migration direction of the sand strips. The circles indicate the lags that correspond with the sand strip wavelength in A or migration velocity in B. These lags are the first peak of the correlation signal of a pixel row and they have to surpass a threshold of 0.3 for the wavelength and 0.6 for the migration velocity. These examples were made by using auto-correlation for the Argus image taken at 9.00 h on 01-04-2008 for A, while B used cross-correlation with the images taken at 9.00 and 10.00 h. One pixel corresponds to 0.5 m.

noticeably different from hours with weak signs. In other words, sand strips developed at all wind velocities above the threshold for aeolian transport to become visible in the Argus imagery and the observed intensity of the transport is strongly governed by the wind direction.

Visual observation of the Argus images provided insight into sand strip development. Firstly, sand strips usually formed at the dune foot and then spread towards the sea with falling tide (Fig. 8). Their initial formation was only close to the waterline when the beach was wide and the wind had a seaward direction, but such conditions were rare. Secondly, sand strips often started out as patches of moving, dry sand that turned into thin strips over time (a few hours), which can also be seen in Kocurek et al. (1992). The length and the width of such a single sand

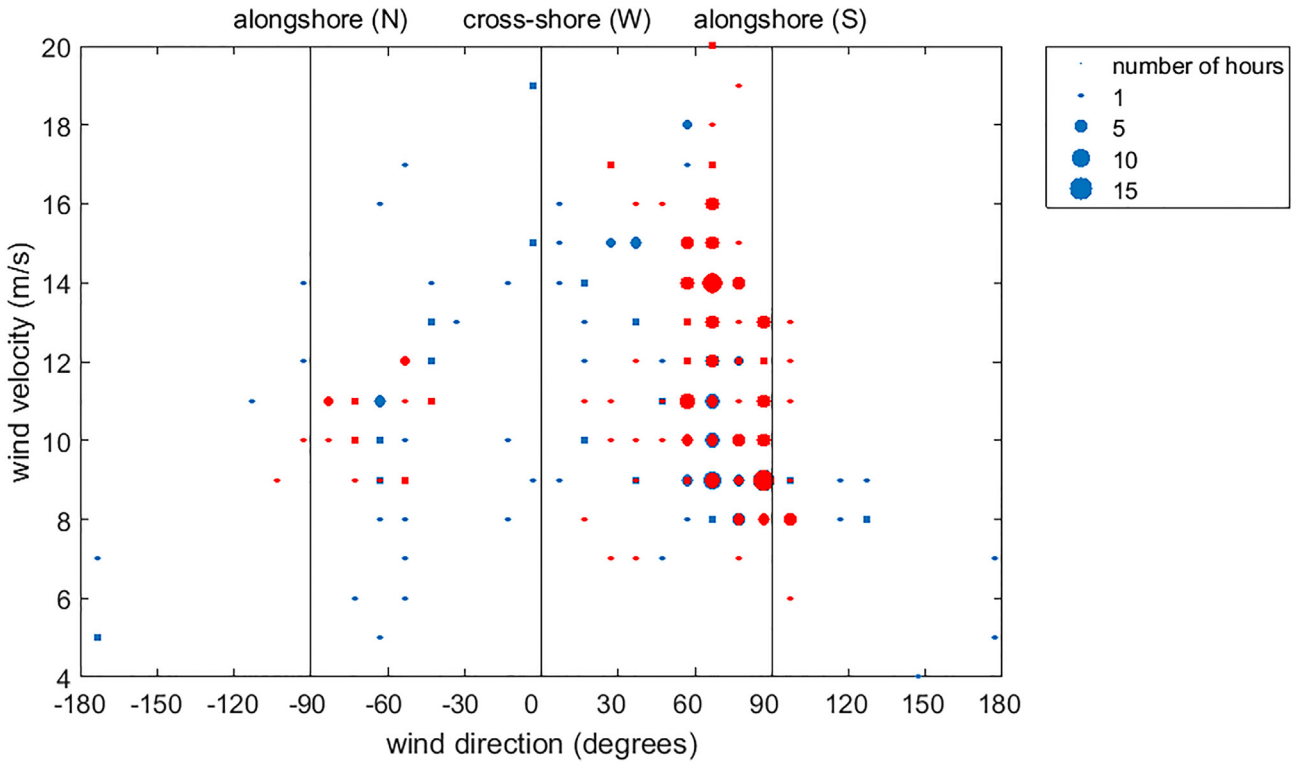

Fig. 7. Wind velocity (m/s) against wind direction (degrees), where 0° is cross-shore from the west, - 90° alongshore from the northern direction and 90° from the southern direction. The blue dots represent hours from October 2011 to March 2012 with any visible trace of aeolian transport. The red dots represent events with strong visual traces of aeolian transport. The total number of observations (hours) that showed signs of aeolian transport is 381, of which 77 were classified as having strong signs of aeolian activity.

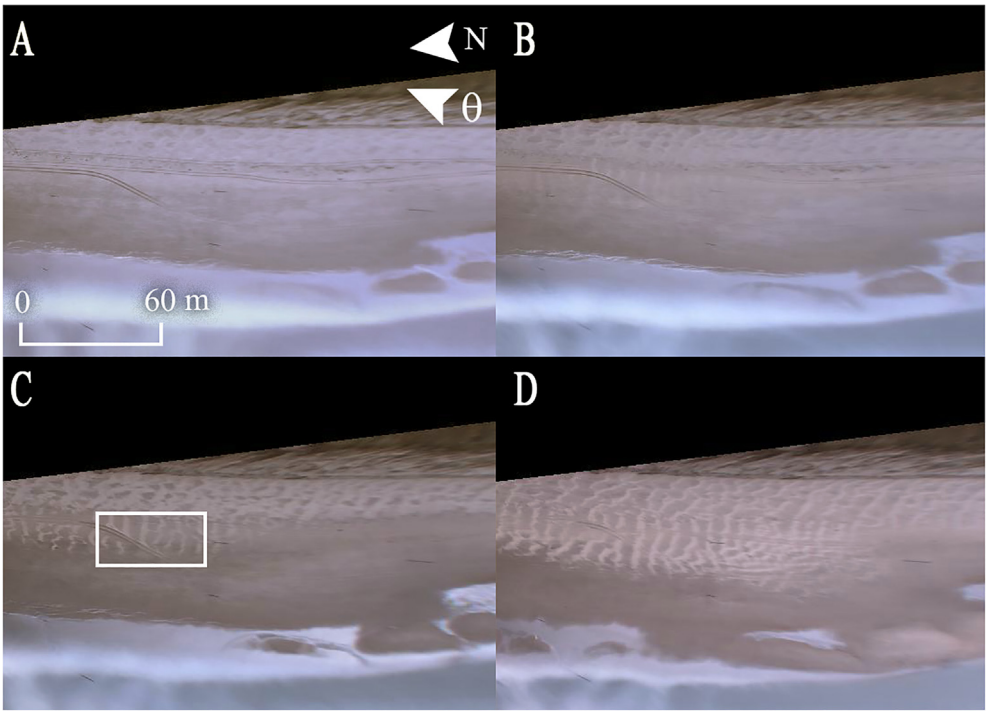

Fig. 8. Development of sand strips, starting with a beach without sand strips (A). An hour later, the beach showed faint traces of aeolian transport close to the dune (B). After another hour, the beach was partly covered with well-developed sand strips (C), and the bedforms spread towards the waterline (D). The images were taken on 07-03-2008 at hourly intervals. The wind speed increased from 9 to 11 m/s and $\theta \approx 67^{\circ}$. $\theta = 0^{\circ}$ is directed cross-shore from the west, $\theta = -90^{\circ}$ alongshore from the north, and $\theta = 90^{\circ}$ alongshore from the south. The dunes, visible by their vegetation, can be found in the east, while the east shows the sea, whose waves have been blurred out by the timex images.

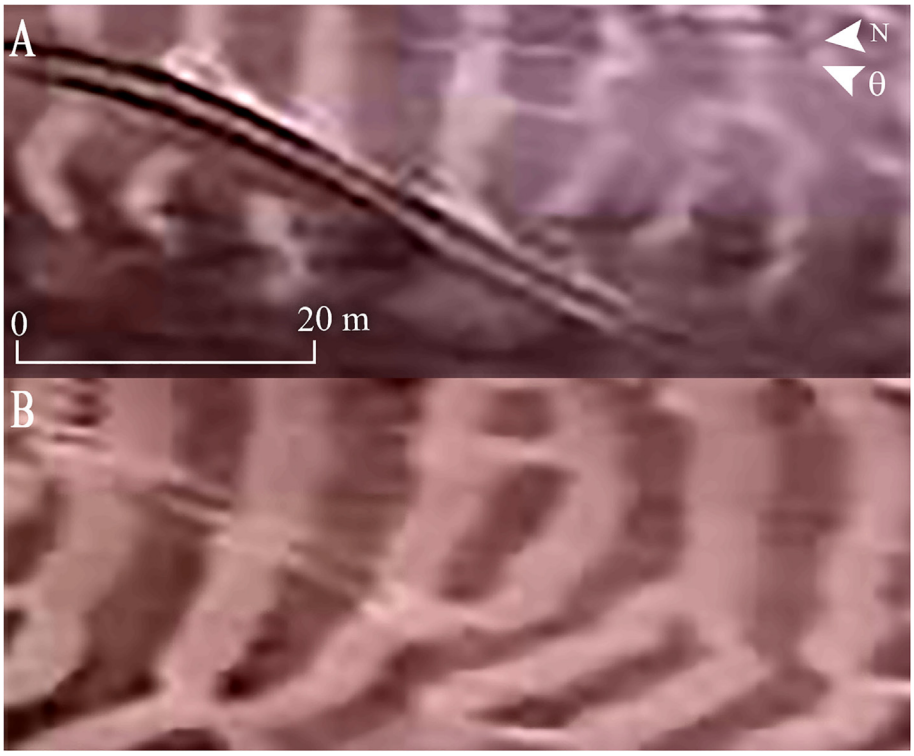

Fig. 9. A section of the beach containing newly developed, relatively narrow and patchy sand strips (A). The sand strips became thicker with time (B), and the strips on the right changed shape. The images were taken on 07-03-2008, 4 h apart. The wind speed and direction were $U \approx 11$ m/s and $\theta \approx 67^{\circ}$. $\theta = 0^{\circ}$ is directed cross-shore from the west, $\theta = -90^{\circ}$ alongshore from the north, and $\theta = 90^{\circ}$ alongshore from the south.

strip grew larger (Fig. 9), but the wavelength usually did not change during this process. Sometimes, when remnant sand strips of an earlier aeolian transport event were present, the new sand strips appeared to have the same shape, size and location of the remnant strips. This changed when the new sand strips began to move.

Several processes cause sand strips to become inactive. The first process takes place when the wind velocity drops below the threshold wind velocity. When this happens, the sand strips remain visible for some time, but they do not move or grow. The second process for sand strip disappearance is the most common: the rising tide stops sand strip

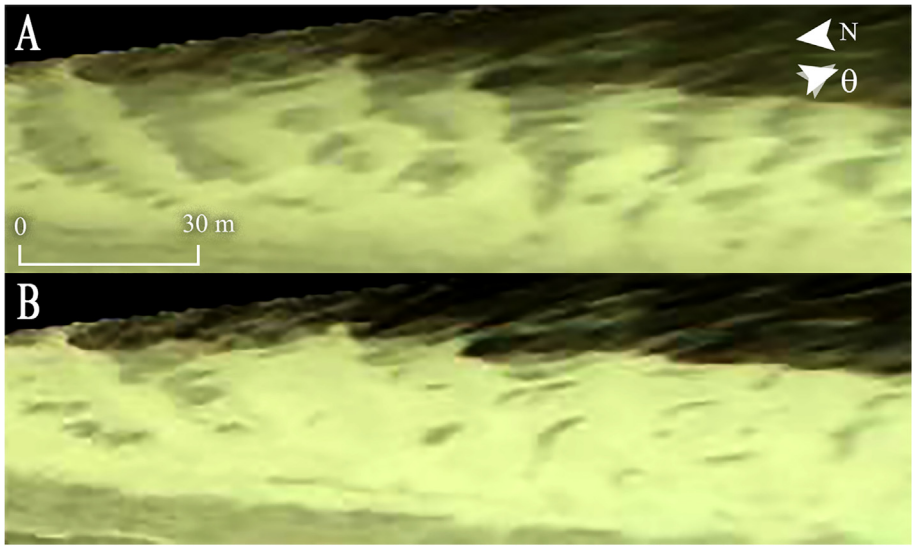

Fig. 10. A beach section with sand strips (A). The bedforms became less distinct with time (B), probably due to drying of the moist, dark sand. The images were taken on 24-07-2007 and are 2 h apart. The wind speed was $U \approx 15$ m/s and θ changed from -73° to -53°. $\theta = 0^{\circ}$ is directed cross-shore from the west, $\theta = -90^{\circ}$ alongshore from the north, and $\theta = 90^{\circ}$ is alongshore from the south.

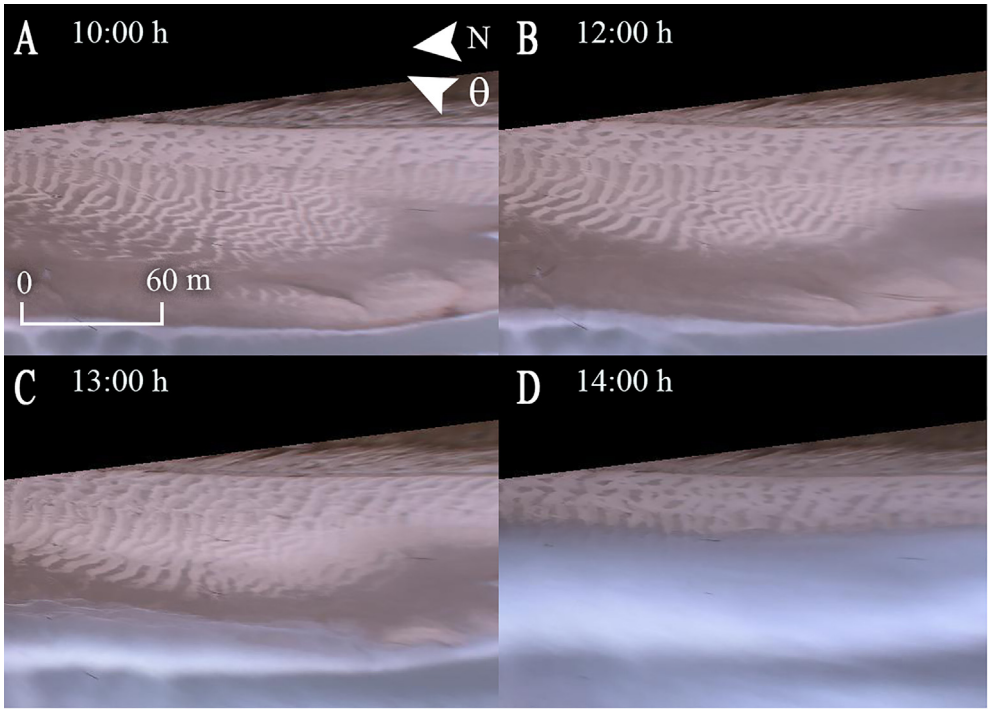

Fig. 11. Sand strips getting washed away by the rising tide. The beach width did not become narrower at first (A to B), but the area with sand strips became smaller. The beach became narrower from (B) to (C), and then at a faster rate from (C) to (D). The images were taken on 07-03-2008 at an hourly interval, except between (A) and (B) which covers a two-hour time gap. The wind speed and direction were $U \approx 12$ m/s and $\theta \approx 67^{\circ}$. $\theta = 0^{\circ}$ is directed cross-shore from the west, $\theta = -90^{\circ}$ alongshore from the north, and $\theta = 90^{\circ}$ alongshore from the south.

activity and, obviously, destroys sand strips present on the intertidal beach (Fig. 11)). Sand strips also disappeared temporarily due to precipitation, but were observed to recover within an hour after a rain event as long as the wind remained above the threshold velocity. Rainfall was not measured at the field site, but the sudden appearance of water droplets on the camera lens and a noticeable darkening of the beach indicated a rain event. A possible third process involves drying of the initially moist sand of the bed, which causes the moist, dark sand to acquire the same colour as the sand strips (Fig. 10). The bedforms may still be there after this drying process, but they are no longer distinguishable in the imagery. However, as one of the possible conditions for sand strip development is wet sand (Nield et al., 2011), it is also feasible that the drying of the sand causes sand strips to decay. In that case, aeolian transport might continue through saltation or creep which cannot be seen by the cameras.

A total of 44 events with well-developed, active sand strips were selected from the 2005–2012 Argus dataset to study their wavelength and migration velocity. Low correlation coefficients (< 0.3) were found for 3 events during the auto-correlation calculations for the sand strip wavelengths. There was 1 event in which the cross-correlation calculations for the sand strip migration velocity remained below 0.6. These events were excluded from the dataset: the number of events with well-

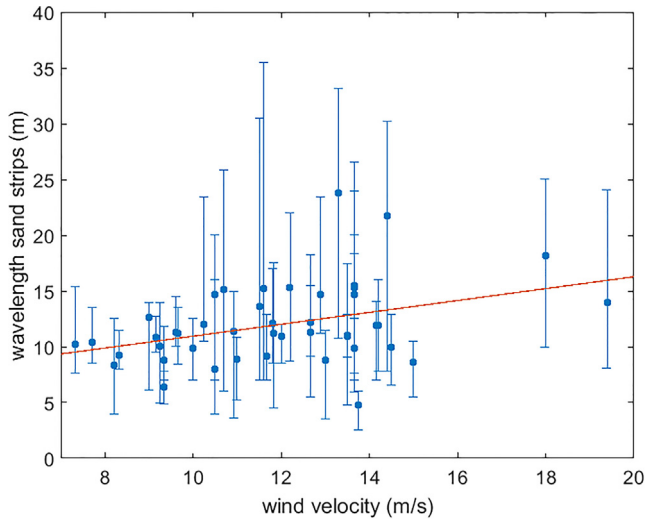

Fig. 12. Sand strip wavelength (m) versus wind velocity (m/s). Each datapoint represents one sand strip event. The corresponding wind velocity has been obtained by averaging the hourly mean wind velocities that were measured at the time the sand strip event took place. The vertical lines represent the 2.5 and 97.5% percentile. The red line is the best fit linear line ($r = 0.38$).

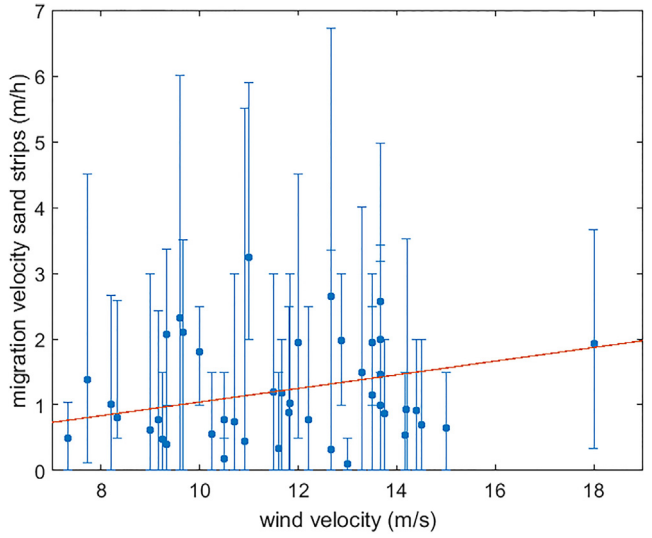

Fig. 13. Sand strip migration velocity (m/h) versus wind velocity (m/s). Each datapoint represents one sand strip event. The corresponding wind velocity has been obtained by averaging the hourly mean wind velocities that were measured at the time the sand strip event took place. The vertical lines represent the 2.5 and 97.5% percentile. The red line is the best fit linear line ($r = 0.32$).

developed, active sand strips was 41 for determining the sand strip wavelength and 43 for the sand strip migration velocities. The analysed imagery resulted in an average sand strip wavelength of 12.0 m with a standard deviation of 2.8 m. A weak, yet statistically significant (at the 95% confidence interval) relationship could be found between the wavelength of the sand strips and the wind velocity ($r = 0.38$, see Fig. 12).

Sand strips moved with an average velocity of 1.24 m/h with a standard deviation of 0.78 m/h. The relationship between the sand strip migration rate and the wind velocity is again weak ($r = 0.32$, $\alpha = 0.05$ Fig. 13), yet statistically significant. Furthermore, it was observed during the selection of the Argus images that sand strips did not necessarily migrate after their formation, or at least not fast enough to be seen by the cameras. Images where this was the case were not selected for further study. If the sand strips did move, their migration did not always happen immediately; the moment of migration ranged from minutes (i.e. the next Argus image) to several hours after sand strip formation. A section of a sand strip was sometimes observed to move faster than other sections. It then disconnected from the rest of the sand strip, only to merge with a sand strip in front of it. This is known as defect repulsion (Kocurek et al., 2010) and can be observed in dunefields (Ewing and Kocurek, 2010; Ewing et al., 2006). The Argus images also showed that sand strips have the tendency to move alongshore, even when the regional wind approached the shoreline at an oblique angle.

5. Discussion

The Egmond Argus video monitoring station has provided a multi-year data set of visual signatures of aeolian transport events. The imagery provides insight into the conditions needed to see visual traces of aeolian transport, even though there is no quantitative data on transport rates.

The average migration velocity for the sand strips 1.24 m/h, which is faster than the sand strip migration velocities found by Nield (2011) (0.176 m/h for real-world beach measurements and 0.39 m/h for simulated bedforms) and for early-stage protodunes (0.32 m/h found by Baddock et al. (2017)). However, our results show a large variability and are based on multiple sand strip events, while Nield (2011) and Baddock et al. (2017) focussed on a single moment of transport.

Not all sand strip development and migration can be seen on Argus images, mostly due to bad visibility, but also because not all transport events may result in sufficient colour contrast between transported and non-transported sand to be used in subsequent analyses. For example, aeolian sand transport over dry sand just in front of the foredune cannot be detected in the imagery.

Dune growth is the result of numerous aeolian events with different transport magnitudes and frequencies. Events with strong winds may result in a high potential transport rate but because their infrequent occurrence may not contribute considerably to long-term aeolian input from the beach to the foredune (Wolman and Miller, 2012; Delgado-Fernandez and Davidson-Arnott, 2011). The results of this research indicate that the wind direction can reduce the impact of (visually) large transport events at this field site even further. Firstly, sand strips were observed when the regional wind was shore-oblique. Therefore, it is possible that only a small fraction of the transported sand will be deposited at the dune foot as the input is proportional to the cosine of the angle of the wind approach from shore normal (Davidson-Arnott and Law, 1996), which is here usually above 60°. Secondly, the steep slope of the foredune is likely to cause the local (on the beach) wind direction to differ from the regional value (Walker et al., 2006; Bauer et al., 2009). The dunes can act as a wall, deflecting oblique winds alongshore. At our site, this is reflected by the alongshore migration of the sand strips, even though the regional wind direction is shore-oblique. This mismatch between the local and regional wind direction will further diminish aeolian input because of the above mentioned cosine effect. Wind velocity is also expected to differ from the regional value and to vary across the beach. In particular, the wind is faster at the waterline (Walker et al., 2006), which may explain why sand strips move at different velocities along the width of the beach, sometimes resulting in sand strip overtaking (e.g. Fig. 14). It should be noted that the difference in migration velocity was not included in our analysis as we focussed on sand strip characteristics on the upper beach. On the whole, our sand strip analysis is thus indicative of substantial differences between local and regional wind characteristics. The common use of regional rather than local wind data in the prediction of long-term

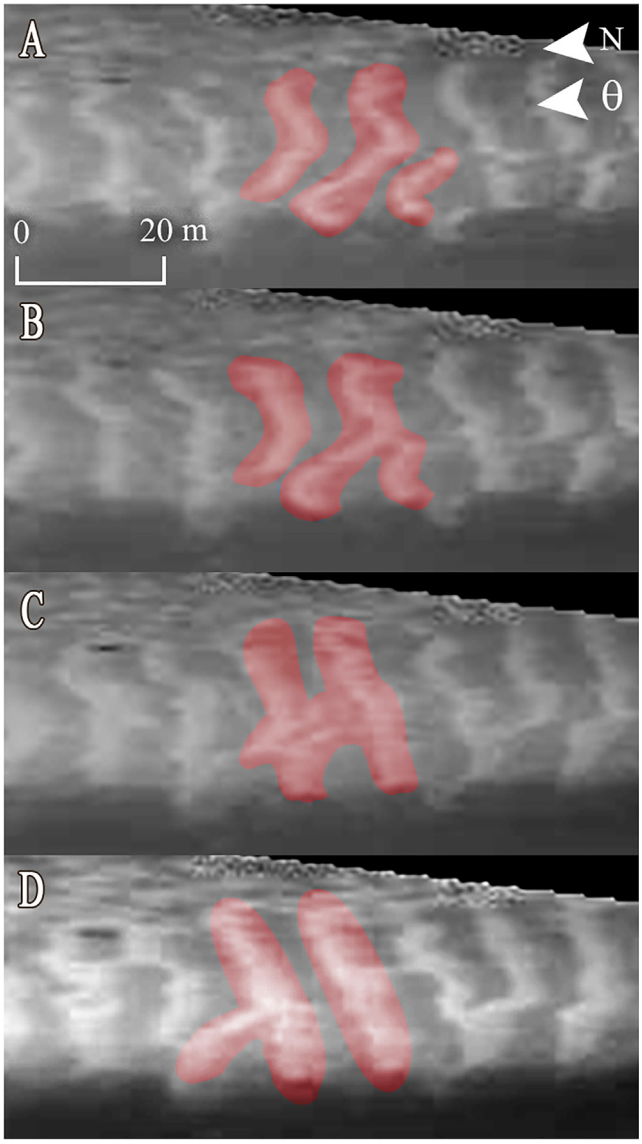

Fig. 14. Rebranching sand strips. The sand strips marked with red were not connected to each other at first (A). Later, one strip connected to the middle one (B), until all sand strips merged together (C), only to turn into separate sand strips again (D). The images were taken on 29-11-2011 at an hourly interval. The wind speed and direction were $U \approx 9$ m/s and $\theta \approx 97^{\circ}$. $\theta = 0^{\circ}$ is cross-shore from the west, $\theta = -90^{\circ}$ is the alongshore wind coming from the north, and $\theta = 90^{\circ}$ is alongshore from the south.

sand deposition on the foredune may thus also contribute to the common overprediction of measured deposition volumes.

6. Conclusion

An Argus video monitoring station has been used to study signs of aeolian sand transport on the beach of Egmond aan Zee, the Netherlands. The transported sand can create low, slipfaceless bedforms, known as sand strips, depending predominantly on the wind direction. Cross-shore winds result in poorly developed sand strips, consisting of only a few patchy stripes of sand. When the wind blows in an (almost) alongshore direction, sand strips form at the dune foot and then the area they cover spreads towards the intertidal area as the tide falls, beginning as patches of dry sand and growing into strips over time. Sand strips disappear when the bed dries or the rising tide washes them away. The average wavelength of sand strips is 12.0 m (with a standard deviation of 2.8 m), while their average migration velocity is 1.24 m/h (with a standard deviation of 0.78 m/h). The migration velocity and wavelength of sand strips are only weakly dependent on the wind velocity ($r = 0.38$ and 0.35, respectively). Sand strips are often oriented alongshore, even though the regional wind is onshore oblique. This suggests substantial wind steering by the steep, 25 m high foredune at the study site.

Acknowledgements

We thank the two referees for their review and various comments on the text. This study was funded by the Dutch Technology Foundation STW (Vici project 13709), which is part of the Netherlands Organisation for Scientific Research (NWO), and which is partly funded by the Ministry of Economic Affairs.

References

ITU-R Recommendation BT.601-7, 2011. Studio encoding parameters of digital television for standard 4: 3 and wide-screen 16: 9 aspect ratios. ITU.
Aagaard, T., Kroon, A., Andersen, S., Srensen, R.M., Quartel, S., Vinther, N., 2005. Intertidal beach change during storm conditions; Egmond, the Netherlands. Mar. Geol. 218 (1), 65–80.
Baas, A.C., Sherman, D.J., 2006. Spatiotemporal variability of aeolian sand transport in a coastal dune environment. J. Coastal Res. 1198–1205.
Baddock, M.C., Nield, J.M., Wiggs, G.F., 2017. Early-stage aeolian protodunes: Bedform development and sand transport dynamics. Earth Surf. Proc. Land.
Bauer, B.O., Davidson-Arnott, R.G.D., Hesp, P.A., Namikas, S.L., Ollerhead, J., Walker, I.J., 2009. Aeolian sediment transport on a beach: surface moisture, wind fetch, and mean transport. Geomorphology 105 (1), 106–116.
Bauer, B.O., Davidson-Arnott, R.G.D., 2002. A general framework for modeling sediment supply to coastal dunes including wind angle, beach geometry, and fetch effects. Geomorphology 49 (1), 89–108.
Bauer, B.O., Davidson-Arnott, R.G.D., 2003. A general framework for modeling sediment supply to coastal dunes including wind angle, beach geometry, and fetch effects. Geomorphology 49 (1), 89–108.
Davidson-Arnott, R.G.D., Bauer, B.O., 2009. Aeolian sediment transport on a beach: thresholds, intermittency, and high frequency variability. Geomorphology 105 (1–2), 117–126.
Davidson-Arnott, R.G.D., Yang, Y., Ollerhead, J., Hesp, P.A., Walker, I.J., 2008. The effects of surface moisture on aeolian sediment transport threshold and mass flux on a beach. Earth Surf. Proc. Land. 33 (1), 55–74.
Davidson-Arnott, R.G., Law, M.N., 1996. Measurement and prediction of long-term sediment supply to coastal foredunes. J. Coastal Res. 654–663.
Davidson-Arnott, R.G., MacQuarrie, K., Aagaard, T., 2005. The effect of wind gusts, moisture content and fetch length on sand transport on a beach. Geomorphology 68 (1), 115–129.
de Winter, R.C., Gongriep, F., Ruessink, B.G., 2015. Observations and modeling of alongshore variability in dune erosion at Egmond aan Zee, the Netherlands. Coast. Eng. 99, 167–175.
Delgado-Fernandez, I., 2010. A review of the application of the fetch effect to modelling sand supply to coastal foredunes. Aeolian Res. 2 (2–3), 61–70.
Delgado-Fernandez, I., Davidson-Arnott, R., 2011. Meso-scale aeolian sediment input to coastal dunes: the nature of aeolian transport events. Geomorphology 126 (1–2), 217–232.
Delgado-Fernandez, I., Davidson-Arnott, R., Ollerhead, J., 2009. Application of a remote sensing technique to the study of coastal dunes. J. Coastal Res. 255 (255), 1160–1167.
Eamer, J.B.R., Walker, I.J., 2010. Quantifying sand storage capacity of large woody debris on beaches using lidar. Geomorphology 118 (1), 33–47.
Edwards, B.L., Namikas, S.L., 2009. Small-scale variability in surface moisture on a fine-grained beach: implications for modeling aeolian transport. Earth Surf. Proc. Land. 34 (10), 1333–1338.
Elbelrhiti, H., 2012. Initiation and early development of barchan dunes: a case study of the Moroccan Atlantic Sahara desert. Geomorphology 138 (1), 181–188.
Enckevort, I.V., Ruessink, B., 2001. Effect of hydrodynamics and bathymetry on video estimates of nearshore sandbar position. J. Geophys. Res.: Oceans 106 (C8), 16969–16979.
Ewing, R., Kocurek, G., 2010. Aeolian dune-field pattern boundary conditions. Geomorphology 114 (3), 175–187.
Ewing, R.C., Kocurek, G., Lake, L.W., 2006. Pattern analysis of dune-field parameters. Earth Surf. Proc. Land. 31 (9), 1176–1191.
Gares, P.A., 1988. Factors affecting eolian sediment transport in beach and dune environments. J. Coastal Res. 121–126 (Special Issue No. 3 Dune/beach interaction).
Guimarães, P.V., Pereira, P.S., Calliari, L.J., Ellis, J.T., 2016. Behavior and identification of ephemeral sand dunes at the backshore zone using video images. Anais da Academia Brasileira de Ciências 88, 1357–1369.
Hage, P.M., 2014. Video Monitoring of Meso-scale Aeolian Activity on a Narrow Beach. Utrecht University (Master's thesis).
Hesp, P.A., Arens, S.M., et al., 1997. Crescentic dunes at schiermonnikoog, the Netherlands. Earth Surf. Proc. Land. 22.

Holland, K.T., Holman, R.A., Lippmann, T.C., Stanley, J., Plant, N., 1997. Practical use of video imagery in nearshore oceanographic field studies. IEEE J. Oceanic Eng. 22 (1), 81–92.
Holman, R., Stanley, J., 2007. The history and technical capabilities of Argus. Coast. Eng. 54 (6–7), 477–491.
Holman, R.A., Sallenger, A.H., 1986. High-energy nearshore processes. Eos, Trans. Am. Geophys. Union 67 (49), 1369.
Hoonhout, B., de Vries, S., 2017. Field measurements on spatial variations in aeolian sediment availability at the Sand Motor mega nourishment. Aeolian Res. 24 (2017), 93–104.
Jackson, N.L., Sherman, D.J., Hesp, P.A., Klein, A.H.F., Ballasteros Jr., F., Nordstrom, K.F., 2006. Small-scale spatial variations in aeolian sediment transport on a fine-sand beach. J. Coastal Res. 1, 379–383 (Special Issue No. 39. Proceedings of the 8th International Coastal Symposium (ICS 2004)).
Jackson, N.L., Nordstrom, K.F., 1997. Effects of time-dependent moisture content of surface sediments on aeolian transport rates across a beach, Wildwood, New Jersey, USA. Earth Surf. Proc. Land. 22 (7), 611–621.
Jackson, N.L., Nordstrom, K.F., 1998. Aeolian transport of sediment on a beach during and after rainfall, Wildwood, NJ, USA. Geomorphology 22 (2), 151–157.
Keijsers, J.G., Poortinga, A., Riksen, M.J., Maroulis, J., 2014. Spatio-temporal variability in accretion and erosion of coastal foredunes in the Netherlands: regional climate and local topography. PloS One 9 (3), e91115.
Kocurek, G., Townsley, M., Yeh, E., Havholm, K.G., Sweet, M.L., 1992. Dune and dune-field development on padre island, texas, with implications for interdune deposition and water-table-controlled accumulation. journal of sedimentary research. Vol. 62 (Kocurek, G., Townsley, M., Yeh, E., Havholm, K.G., Sweet, M.L., 1992, Dune and Dune-Field Development on Padre Island, Texas, with Implications for Interdune Deposition and Water-Table-Controlled Accumulation: Journal of Sedimentary Research, v. Vol.), pp. 622–635.
Kocurek, G., Ewing, R.C., Mohrig, D., 2010. How do bedform patterns arise? New views on the role of bedform interactions within a set of boundary conditions. Earth Surface Processes Landforms 35 (1), 51–63.
Lippmann, T.C., Holman, R.A., 1989. Quantification of sand bar morphology: a video technique based on wave dissipation. J. Geophys. Res.: Oceans 94 (C1), 995–1011.
Masselink, G., Kroon, A., Davidson-Arnott, R., 2006. Morphodynamics of intertidal bars in wave-dominated coastal settings – a review. Geomorphology 73 (1), 33–49.
McKenna Neuman, C., Langston, G., 2006. Measurement of water content as a control of particle entrainment by wind. Earth Surf. Proc. Land. 31 (3), 303–317.
Miot da Silva, G., Hesp, P., 2010. Coastline orientation, aeolian sediment transport and foredune and dunefield dynamics of Moçambique Beach, Southern Brazil. Geomorphology 120 (3-4), 258–278.
Nield, J.M., 2011. Surface moisture-induced feedback in aeolian environments. Geology 39 (10), 915–918.
Nield, J.M., Wiggs, G.F., 2011. The application of terrestrial laser scanning to aeolian saltation cloud measurement and its response to changing surface moisture. Earth Surf. Proc. Land. 36 (2), 273–278.
Nield, J.M., Wiggs, G.F.S., Squirrell, R.S., 2011. Aeolian sand strip mobility and proto-dune development on a drying beach: examining surface moisture and surface roughness patterns measured by terrestrial laser scanning. Earth Surf. Proc. Land. 36 (4), 513–522.
Nield, J.M., King, J., Wiggs, G.F.S., Leyland, J., Bryant, R.G., Chiverrell, R.C., Darby, S.E., Eckardt, F.D., Thomas, D.S.G., Vircavs, L.H., Washington, R., 2013. Estimating aerodynamic roughness over complex surface terrain. J. Geophys. Res. Atmos. 118 (23), 12948–12961.
Nield, J.M., King, J., Jacobs, B., 2014. Detecting surface moisture in aeolian environments using terrestrial laser scanning. Aeolian Res. 12, 9–17.
Pianca, C., Holman, R., Siegle, E., 2015. Shoreline variability from days to decades: Results of long-term video imaging. J. Geophys. Res.: Oceans 120 (3), 2159–2178.
Quartel, S., Grasmeijer, B.T., 2007. Dynamiek van het strand bij Noordwijk aan Zee en Egmond aan Zee en het effect van suppleties. Rijksinstituut voor Kust en Zee (RIKZ). Opdracht RKZ-1667, (september 2006).
Quartel, S., Ruessink, B., Kroon, A., 2007. Daily to seasonal cross-shore behaviour of quasi-persistent intertidal beach morphology. Earth Surf. Proc. Land. 32 (9), 1293–1307.
Ruessink, B.G., Pape, L., Turner, I.L., 2009. Daily to interannual cross-shore sandbar migration: observations from a multiple sandbar system. Cont. Shelf Res. 29 (14), 1663–1677.
Sherman, D.J., Hotta, S., 1990. Aeolian sediment transport: theory and measurement. Coastal Dunes: Form and Process 17, 37.
Sherman, D.J., Houser, C., Baas, A.C.W., 2013a. Electronic Measurement Techniques for Field Experiments in Process Geomorphology. Elsevier Ltd. volume 14.
Sherman, D.J., Li, B., 2012. Predicting aeolian sand transport rates: a reevaluation of models. Aeolian Res. 3 (4), 371–378.
Sherman, D.J., Jackson, D.W., Namikas, S.L., Wang, J., 1998. Wind-blown sand on beaches: an evaluation of models. Geomorphology 22 (2), 113–133.
Sherman, D.J., Li, B., Farrell, E.J., Ellis, J.T., Cox, W.D., Maia, L.P., Sousa, P.H.G.O., 2011. Measuring aeolian saltation: a comparison of sensors. J. Coastal Res. 59 (May 2017), 280–290.
Sherman, D.J., Houser, C., Ellis, J.T., Farrell, E.J., Li, B., Davidson-Arnott, R.G., Baas, A.C., Maia, L.P., 2013b. Characterization of aeolian streamers using time-average videography. J. Coastal Res. 165 (65), 1331–1336.
Svasek, J.N., Terwindt, J.H.J., 1974. Measurements of sand transport by wind on a natural beach. Sedimentology 21 (2), 311–322.
Udo, K., Kuriyama, Y., Jackson, D.W., 2008. Observations of wind-blown sand under various meteorological conditions at a beach. J. Geophys. Res.: Earth Surface 113 (F4).
van Enckevort, I.M.J., Ruessink, B.G., Coco, G., Suzuki, K., Turner, I.L., Plant, N.G., Holman, R.A., 2004. Observations of nearshore crescentic sandbars. J. Geophys. Res. C: Oceans 109 (6), 1–17.
Walker, I.J., Hesp, P.A., Davidson-Arnott, R.G.D., Ollerhead, J., 2006. Topographic steering of alongshore airflow over a vegetated foredune: greenwich dunes, Prince Edward Island, Canada. J. Coastal Res. 225 (225), 1278–1291.
Wiggs, G., Atherton, R., Baird, A., 2004. Thresholds of aeolian sand transport: establishing suitable values. Sedimentology 51 (1), 95–108.
Wijnberg, K.M., Terwindt, J.H.J., 1995. Extracting decadal morphological behaviour from high-resolution, long-term bathymetric surveys along the Holland coast using eigenfunction analysis. Mar. Geol. 126 (1–4), 301–330.
Wolman, M.G., Miller, J.P., 2012. Fluvial processes in geomorphology. Courier Corporation.